iScience

CellPress
OPEN ACCESS

Article

Matrix-assisted laser desorption ionization mass spectrometry profiling of plasma exosomes evaluates osteosarcoma metastasis

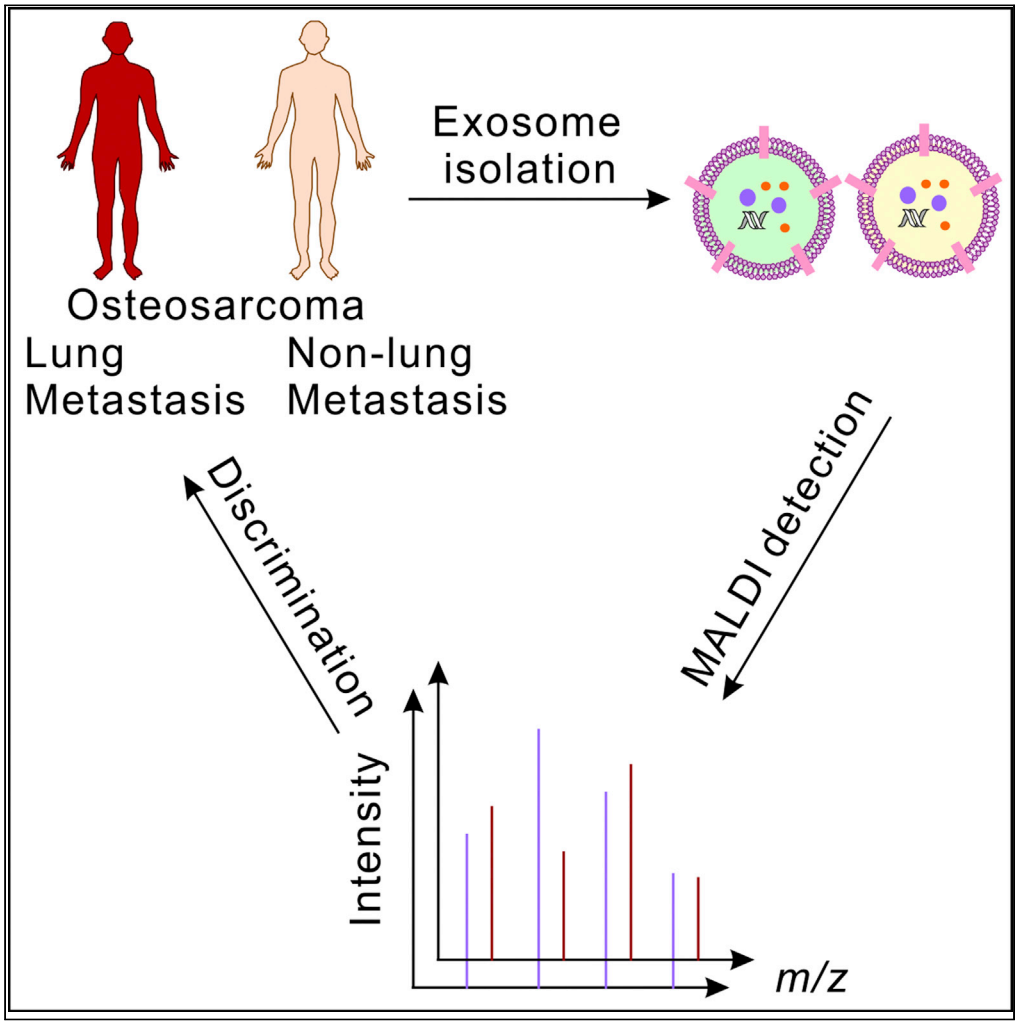

Zhenzhen Han, Cheng Peng, Jia Yi, ..., Shuping Long, Liang Qiao, Yuhui Shen

liang_qiao@fudan.edu.cn (L.Q.)
yuhuiss@163.com (Y.S.)

Highlights

MALDI-TOF profiling of plasma-derived exosomes can identify osteosarcomas

The method can discriminate osteosarcoma lung metastasis from non-lung metastasis

Seven exosomal proteins were identified as potential biomarkers of lung metastasis

Han et al., iScience *24*, 102906
August 20, 2021
https://doi.org/10.1016/j.isci.2021.102906

iScience

CellPress
OPEN ACCESS

Article

Matrix-assisted laser desorption ionization mass spectrometry profiling of plasma exosomes evaluates osteosarcoma metastasis

Zhenzhen Han,[1,2,4] Cheng Peng,[1,4] Jia Yi,[2] Yiwen Wang,[2] Qi Liu,[1] Yi Yang,[2] Shuping Long,[3] Liang Qiao,[2,5,*] and Yuhui Shen[1,*]

SUMMARY

Osteosarcoma is the most common primary sarcoma of bone among adolescents, often characterized by early lung metastasis resulting in high mortality. Recently, exosomes have been used in liquid biopsy to monitor tumors. Herein, we used matrix-assisted laser desorption/ionization time-of-flight mass spectrometry (MALDI-TOF MS) to profile human plasma exosomes for the evaluation of osteosarcoma lung metastasis. Forty patients with osteosarcoma with (n = 20) or without (n = 20) lung metastasis as well as 12 heathy controls were recruited. Exosomes were isolated from human plasma for MALDI-TOF MS analysis. Multivariate statistical analyses were performed based on the MALDI-TOF mass spectra. The strategy can efficiently differentiate osteosarcomas from healthy controls and further discriminate osteosarcoma lung metastasis from non-lung metastasis. We identified seven exosomal proteins as potential biomarkers of osteosarcoma lung metastasis. The proposed method holds great promise to clinically diagnose osteosarcoma and monitor osteosarcoma lung metastasis.

INTRODUCTION

Osteosarcoma is the most common primary sarcoma of bone, particularly among young children and teenagers (Behjati et al., 2017). Although the survival rate of patients with osteosarcoma has been improved to ~70% by surgery combined with adjuvant chemotherapy (Kansara et al., 2014), still about 20% of patients with osteosarcoma suffer from metastases (Meyers et al., 2011), among which more than 85% metastatic lesion is detected in the lungs (Bielack et al., 2014). The early diagnosis of osteosarcoma lung metastasis is crucial for the treatment and prognosis of osteosarcoma. Computed tomography (CT) scanning combining histopathologic biopsy is usually used to diagnose osteosarcoma lung metastasis, but is less efficient in the detection of small lesions (Luetke et al., 2014). Moreover, the traditional biopsy methods require complex operations, which are highly invasive and have the risk of arousing tumor spread (Brock et al., 2015).

As an alternative diagnosis method, liquid biopsy is emerging in recent years. The liquid biopsy involving exosomes has recently been reported to monitor tumor progression (Gerlinger et al., 2012) and long-term treatment response (Liu et al., 2020). Exosomes exhibit the size of 30 nm–150 nm, containing nucleic acids, lipids, proteins, *etc.* They are shed by almost all types of cells and found in various body fluids, such as plasma, urine, breast milk, saliva, *etc.* (Chen et al., 2018; Costa-Silva et al., 2015; Di et al., 2019; Tieu et al., 2020; Yang et al., 2020). Exosomes play an important role in cellular communication, signal transduction and immune response and serve as potential biomarkers for various diseases (Jansen et al., 2009; Saenz-Pipaon et al., 2020). The implications of exosomes in osteosarcoma have also been studied. It has been reported that osteosarcoma-derived exosomes can work as transfer cargo and are relevant with tumor progression and metastasis (Chicon-Bosch and Tirado, 2020; Galardi et al., 2019). To date, the most widely used platforms (Witwer et al., 2013) to characterize exosomes (see Table S1) include 1) dynamic light scattering (DLS) (Palmieri et al., 2014), nanoparticle tracking analysis (NTA) (Gardiner et al., 2013) and tunable resistive pulse sensing (TRPS) (Vogel et al., 2016) for size characterization; 2) Western blot (Rat et al., 2008), enzyme-linked immunosorbent assay (ELISA) (Hoshino et al., 2020) and nano-flow cytometry (Welsh et al., 2020) for subgroup characterization; 3) mass spectrometry for proteomic characterization (Andaluz Aguilar et al., 2020; Hoshino et al., 2020); and 4) sequencing for genomic and transcriptomic

[1]Department of Orthopedics, Ruijin Hospital, Shanghai Jiao Tong University School of Medicine, Shanghai 200000, China

[2]Department of Chemistry, Fudan University, Shanghai 200433, China

[3]Department of Clinical Laboratory Medicine, Shanghai Tenth People's Hospital of Tongji University, Shanghai, China

[4]These authors contributed equally

[5]Lead contact

*Correspondence: liang_qiao@fudan.edu.cn (L.Q.), yuhuiss@163.com (Y.S.)

https://doi.org/10.1016/j.isci.2021.102906

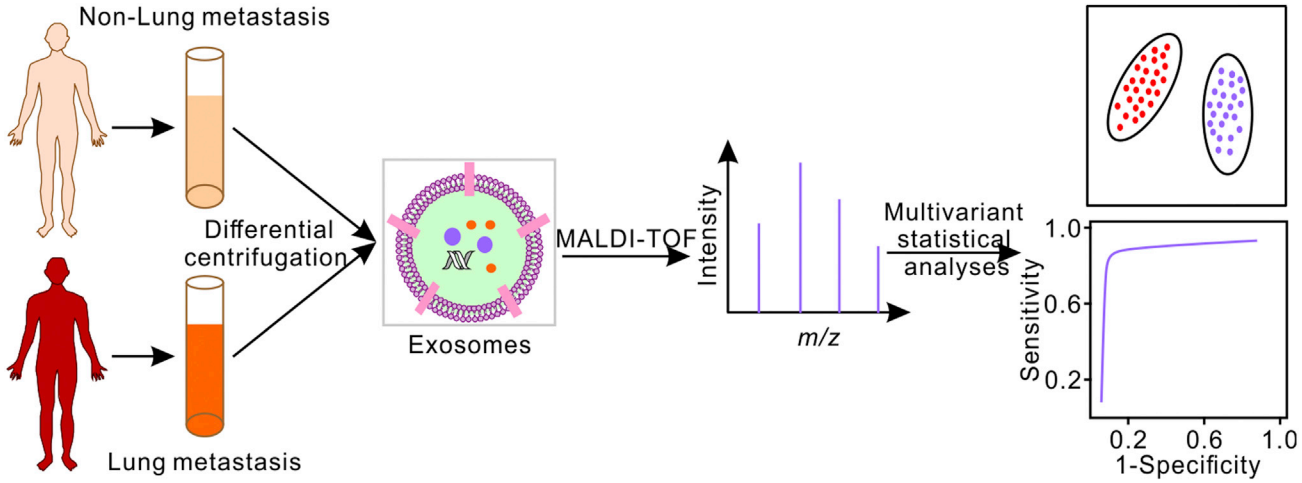

Scheme 1. Schematic illustration of the MALDI-TOF MS profiling of plasma exosomes for the evaluation of osteosarcoma lung metastasis

characterization (Morhayim et al., 2017; Yang et al., 2017a). These methods can provide the phenotype and biological information of exosomes but suffer from complex operation, time-consuming preparation and high requirements on instruments, which limit further clinical application.

Matrix-assisted laser desorption/ionization time-of-flight mass spectrometry (MALDI-TOF MS) has attracted increasing interests in clinical diagnosis with its high throughput, low sample consumption, label-free and direct analysis ability, easy operation, and low cost per sample characterization (Jagadeesan and Ekstrom, 2017; Rathore et al., 2008). It has been used to identify bacterial pathogens by mass fingerprinting for clinical usage (Varadi et al., 2017; Yi et al., 2018, 2019) and determine treatment benefit from epidermal growth factor receptor inhibitors in patients with non-small cell lung cancer as a laboratory-developed clinical test (Butts, 2014). It has also shown great potential in screening of Alzheimer's disease (Nakamura et al., 2018), rapid diagnosis and treatment monitoring of active *Mycobacterium tuberculosis* (TB) disease (Liu et al., 2017), and detection of COVID-19 (Yan et al., 2021). Recently, it has been further utilized for the detection and analysis of exosomes. Stübiger et al. used MALDI-TOF MS to demonstrate the differential expression of proteins in extracellular vesicles (EVs) of different parental cells with an increasing chemoresistance (Stübiger et al., 2018). Singhto et al. applied MALDI-TOF MS to discriminate the urinary exosomes from microvesicles (Singhto et al., 2019). Lin et al. demonstrated that MALDI-TOF MS can identify urinary EVs proteins, *i.e.,* alpha 1-antitrypsin and histone H2B1K, for the diagnosis and prognosis of urothelial carcinoma (Lin et al., 2016). Nguyen et al. proved the platelet factor 4 as a biomarker of exosomes from human plasma by MALDI-TOF MS (Nguyen et al., 2019). Zhu et al. used MALDI-TOF MS to diagnose melanoma and explore the disease progression (Zhu et al., 2019b).

In this study, we demonstrate that MALDI-TOF MS profiling of plasma exosomes can be used to evaluate osteosarcoma lung metastasis (Scheme 1). We first analyzed the exosomes from normal osteoblast cells and osteosarcoma cells and found that the mass fingerprints of exosomes can better resolve different cells than the mass fingerprints of the cells themselves. Then, mass fingerprints of plasma-derived exosomes from patients with osteosarcoma with/without lung metastasis (n = 20 each) as well as healthy controls (n = 12) were collected. The plasma-derived exosomes from patients with osteosarcoma can be well distinguished from healthy controls by principal component analysis (PCA) and hierarchical clustering analysis of their MALDI-TOF mass spectra. The method can further discriminate osteosarcomas with lung metastasis from those without lung metastasis. Combining machine learning methods and LC-MS/MS-based proteomic analysis, we identified seven exosomal proteins from the MALDI-TOF mass spectra of osteosarcoma lung metastasis as potential biomarkers. These results demonstrated that the MALDI-TOF MS profiling of exosomes can be used for the diagnosis, treatment, and prognosis of osteosarcoma, with the advantages of rapid assay, high-throughput, low sample consumption, label-free, and low cost.

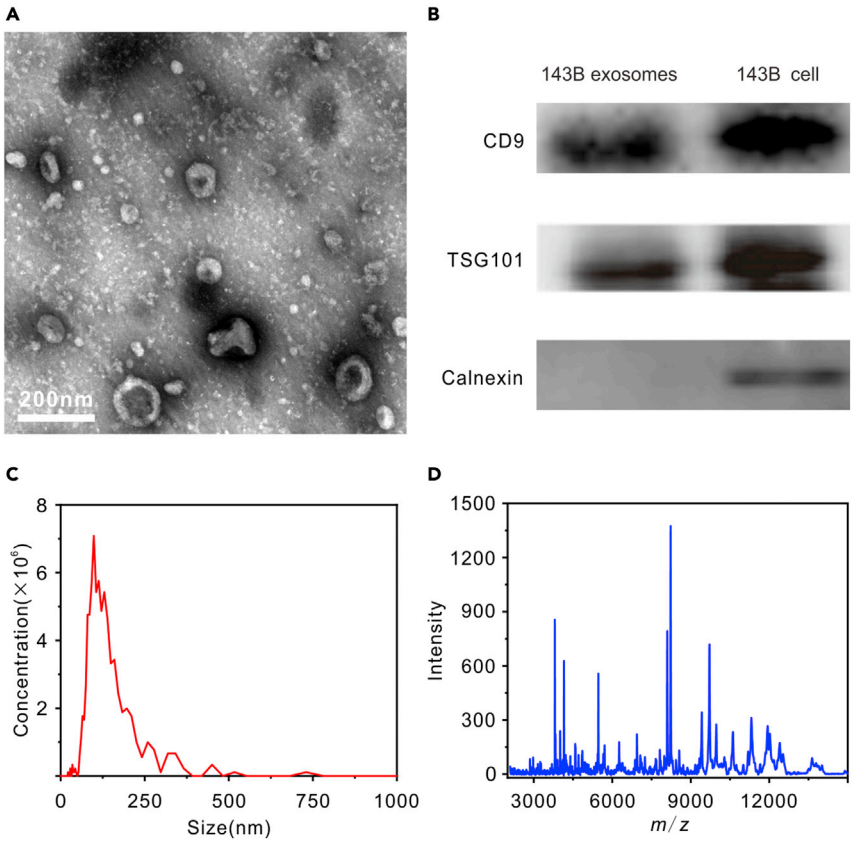

Figure 1. Characterization of exosomes isolated from 143B osteosarcoma cell culture medium
(A–D) (A) TEM micrographs, (B) Western blot analysis of exosome markers, (C) NTA measurement (1000-times dilution), and (D) MALDI-TOF MS fingerprints in the range *m/z* 2000–15,000. Scale bar: 200 nm.

RESULTS

MALDI-TOF profiling of exosomes to distinguish different cells

Exosomes isolated from 143B osteosarcoma cells were used as model samples to illustrate the proposed method. First, exosomes were separated from 143B cell culture medium through differential centrifugation and then characterized by transmission electron microscopy (TEM). As shown in Figure 1A, typical cup-shaped exosomes can be observed in accordance with previous report (Jerez et al., 2017). The isolated exosomes were further characterized by Western blot for exosome-associated biomarkers, as well as by NTA for size distribution. As shown in Figure 1B, the exosomes were positive for CD9 and TSG101 biomarkers, while calnexin, a negative biomarker, only existed in cell lysate. As shown in Figure 1C, the exosomes had a homogeneous size distribution with an average diameter of 120 $\pm$ 11 nm.

Subsequently, MALDI-TOF MS methods were optimized for profiling the exosomes. Sinapic acid (SA) was a more suitable MALDI matrix for exosome characterization than 2,5-dihydroxybenzoic acid (DHB) and α-cyano-4-hydroxycinnamic acid (HCCA), as illustrated in Figure S1. MALDI-TOF mass spectrum of 143B osteosarcoma-cells-derived exosomes was acquired in the mass-to-charge (*m/z*) range 2000–15,000, as shown in Figure 1D. As shown in Figure S2, the mass spectra across batches were highly consistent, demonstrating the sound stability of MALDI-TOF MS platform.

Then, MALDI-TOF mass spectra of exosomes isolated from the normal osteoblast cells (3T3E1) and the osteosarcoma cells (143B, HOS, MG63 and U2OS) are presented in Figure 2A. It can be observed that each type of exosomes has its own characteristic mass fingerprints. For example, the mass spectrum of 3T3E1 exosomes had four strong specific peaks at *m/z* = 4964, 9969, 10,958, and 11,314. The mass spectrum of 143B exosomes had eight strong specific peaks at *m/z* = 3805, 4153, 5468, 8102, 8230, 9422, 9715, and

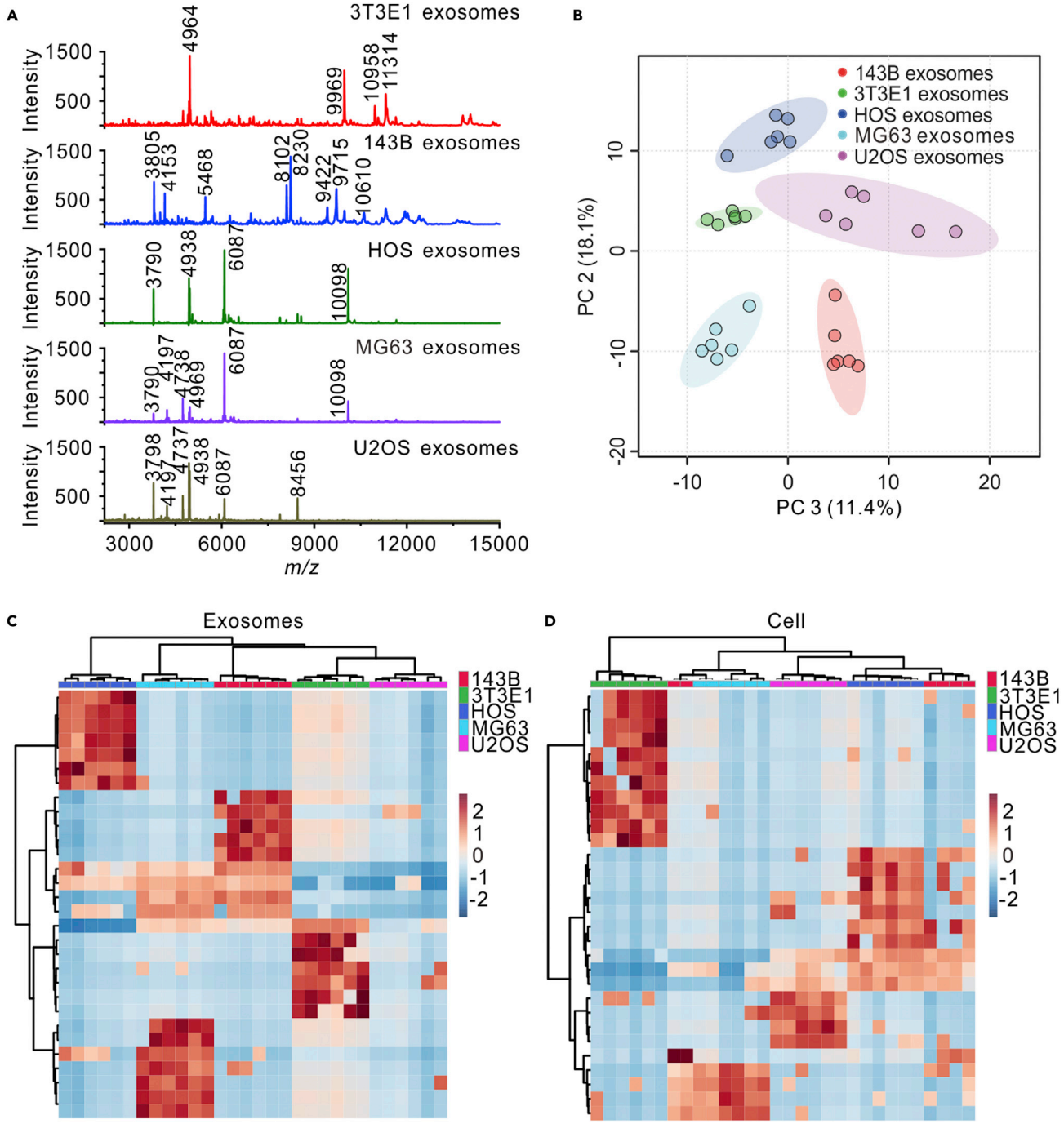

Figure 2. MALDI-TOF mass spectra of exosomes derived from different cell lines and PCA and hierarchical clustering of the MALDI mass spectra

(A) MALDI-TOF mass spectra of exosomes from 3T3E1, 143B, HOS, MG63, and U2OS cells. Main peaks of exosomes were labeled in the figures.

(B–D) (B) PCA of the MALDI-TOF mass spectra obtained from 3T3E1, 143B, HOS, MG63, and U2OS exosomes. Hierarchical clustering results of 3T3E1, 143B, HOS, MG63, and U2OS cell lines based on the MALDI-TOF mass spectra of (C) exosomes or (D) cells, shown as heatmap using Euclidean distance measure and Ward linkage. For MALDI-TOF analyses, six replicates were performed on each cell line.

10,610. The mass spectrum of HOS exosomes showed strong specific peaks at *m/z* = 3790, 4938, 6087, and 10,098. The mass spectrum of MG63 exosomes showed strong specific peaks at *m/z* = 4197, 4738, and 4969. The mass spectrum of U2OS exosomes showed strong specific peaks at *m/z* = 3798, 4737, 4938, and 8456. The mass fingerprints of 3T3E1 exosomes and 143B exosomes were very different from the other

osteosarcoma exosomes. HOS exosomes, MG63 exosomes, and U2OS exosomes had identical and differential peaks. For comparison, MALDI-TOF mass spectra of different cells were also collected and are shown in Figure S3A. It was observed that all the osteosarcoma cells shared similar mass fingerprints.

The mass fingerprints of different exosomes and cells were analyzed by PCA and hierarchical clustering, as shown in Figures 2B, S3B, 2C, and 2D. As shown in Figure 2B, the mass spectra of different exosomes can be clearly grouped into five sets and completely distinguished by PCA. In the Figure S3B, the mass spectra of different cells cannot be well distinguished. The hierarchical clustering heatmaps are displayed in Figures 2C and 2D. The mass spectra of exosomes derived from same cells were classified into same clusters. However, on the cell level, the data of 143B cells were wrongly clustered. All of these results demonstrated that MALDI-TOF mass spectra of exosomes can better discriminate different cells than those of the whole cell. We have also performed the hierarchical clustering combining the MALDI-TOF mass spectra of exosomes and cells. As shown in Figure S4, all the cells were clustered together. The exosomes from HOS, 143B and MG63 were clustered together. The exosomes from 3T3E1 and U2OS were clustered together and closer to the cells than the other exosomes. Nevertheless, even for 3T3E1 and U2OS, the mass fingerprints of the cells were more similar to the other cells than the corresponding exosomes. The results suggest that the mass spectra differences between biological entities are more significant than those among the cells of origin.

Identification of osteosarcomas by MALDI-TOF profiling of exosomes

Based on the success in the cell model, the MALDI-TOF profiling of exosomes was applied to real clinical samples (Table S2). Plasma-derived exosomes were isolated from patients with osteosarcoma and healthy controls and then characterized by NTA, TEM, and Western Blot. As shown in Figure S5, the exosomes isolated from patients with osteosarcoma and healthy controls were typical cup-shaped, positive for CD63, CD9, and CD81, and had a homogeneous size distribution with an average diameter of 120 $\pm$ 10 nm. Figure 3A shows the representative exosome mass fingerprints of a patient and a healthy volunteer. Their fingerprint spectra were significantly different in the mass range of *m/z* 2000 to 20,000. PCA was performed to the MALDI-TOF mass spectra of plasma-derived exosomes from 12 patients with osteosarcoma and 12 healthy controls. The peak intensity matrix of all the samples is listed in the Data S1, which is derived from the raw data after data preprocessing and peak alignment by MALDIquant (Gibb and Strimmer, 2012). As shown in Figure 3B, healthy volunteers and patients with osteosarcoma can be clearly classified into two sets in score plots of PCA based on the mass spectra of exosomes. Hierarchical clustering was also used to analyze the mass fingerprints of the exosomes. As shown in Figure S6, hierarchical clustering indicated that the patients with osteosarcoma can be well distinguished from the healthy controls. Then, partial least squares-discriminant analysis (PLS-DA), a supervised classification method, was applied to find out the distinctive features on the exosomal mass fingerprints between patients with osteosarcoma and healthy volunteers (Figure 3C). Thirty-two peaks with variable importance in the projection (VIP) value >1.5 were considered as potential biomarkers.

To demonstrate whether the MALDI-TOF profile difference between patients with osteosarcoma and healthy controls is osteosarcoma-specific or cancer-specific, we have collected the plasma of five patients with lung cancer. Exosomes were isolated from the plasma samples and then characterized by MALDI-TOF MS. Figure S7A shows a representative mass spectrum of plasma-derived exosomes from a patient with lung cancer. PCA was performed on the MALDI-TOF mass spectra of the plasma-derived exosomes from 12 patients with osteosarcoma, 12 healthy controls, and 5 patients with lung cancer. As shown in Figure S7B, the mass spectra of exosomes can be clearly classified into three sets, i.e., healthy controls, patients with osteosarcoma, and patients with lung cancer. Hierarchical clustering was also used to analyze the mass spectra of the exosomes. As shown in Figure S7C, hierarchical clustering indicated that the patients with osteosarcoma or patients with lung cancer can be well distinguished from the healthy controls, and patients with osteosarcoma can also be distinguished from patients with lung cancer. The distance between the different types of cancer is significantly smaller than the distance between patients with cancer and healthy controls. Therefore, the exosomes from patients with cancer were significantly different in MALDI-TOF mass spectra compared with those from healthy volunteers, while the exosomes from patients with different kinds of cancer were also different in MALDI-TOF mass spectra.

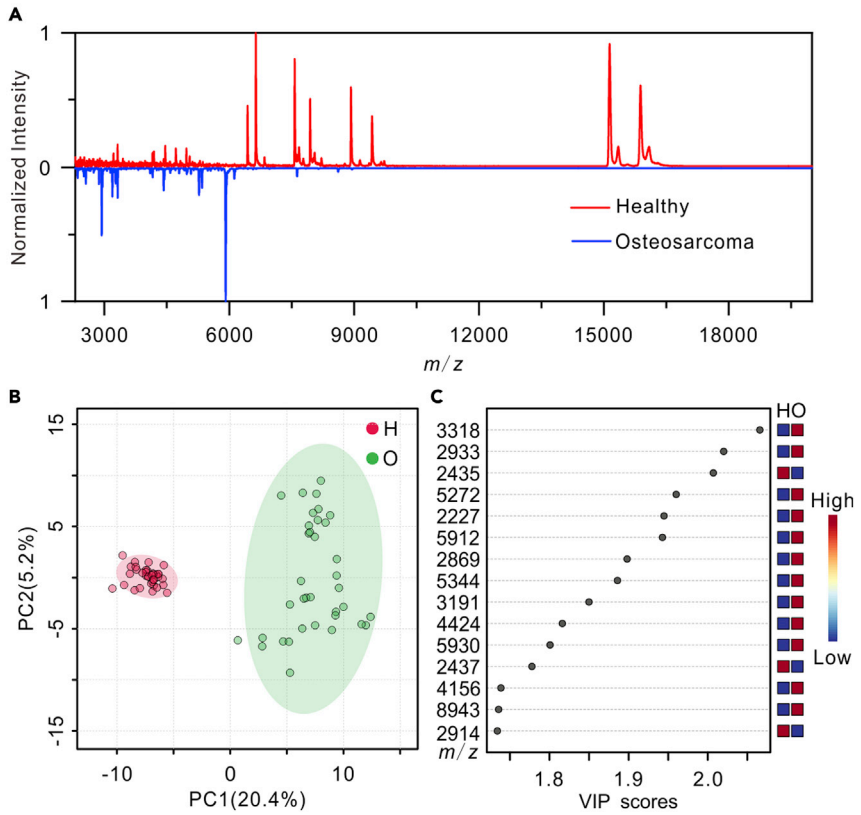

Figure 3. MALDI-TOF mass spectra of plasma-derived exosomes for the identification of osteosarcoma

(A) MALDI-TOF mass spectra of plasma-derived exosomes isolated from a patient with osteosarcoma and a healthy volunteer.

(B) PCA of the MALDI-TOF data of plasma-derived exosomes isolated from 12 healthy controls (H) and 12 patients with osteosarcoma (O).

(C) Important MALDI-TOF MS features of plasma-derived exosomes from the 12 patients with osteosarcoma (O) compared with the 12 healthy volunteers (H) identified by PLS-DA. For MALDI-TOF analyses, three replicates were performed on each sample.

Identification of osteosarcoma lung metastasis

With the success on the classification of patients with osteosarcoma from healthy controls, we further studied the possibility of using MALDI-TOF MS profiling of plasma-derived exosomes for the evaluation of osteosarcoma lung metastasis. Plasma-derived exosomes isolated from 10 patients with osteosarcoma non-lung metastasis and 10 patients with lung metastasis (Table S2) were measured by NTA, TEM, Western blot, and MALDI-TOF MS. As shown in Figure S5, the exosomes were typical cup-shaped, positive for CD63, CD9, and CD81, and had a homogeneous size distribution with an average diameter of around 120 $\pm$ 6 nm. Figure 4A shows the representative MALDI-TOF MS fingerprints of plasma-derived exosomes from a patient with osteosarcoma lung metastasis and a patient with non-lung metastasis. The fingerprint spectra are clearly different in the range of *m/z* 2000 to 20,000. By PCA classification, the mass spectra of plasma-derived exosomes from the patients with osteosarcoma non-lung metastasis and patients with lung metastasis can be separated into two discriminative groups, shown in Figure 4B. As shown in Figure S8, the hierarchical clustering can also classify the patients with osteosarcoma lung metastasis and patients with non-lung metastasis based on the mass spectra. The results demonstrated the potential of MALDI-TOF profiling of plasma-derived exosomes for the diagnosis of osteosarcoma lung metastasis.

To find out the potential biomarkers of osteosarcoma lung metastasis, PLS-DA was performed on the MALDI-TOF mass spectra of plasma-derived exosomes from the patients with 10 osteosarcoma non-lung metastasis and the 10 patients with lung metastasis. Figure 4C lists the VIP of top 15 features, representing the contribution of each feature to the PLS-DA model, and there were 33 peaks with VIP value >1.5,

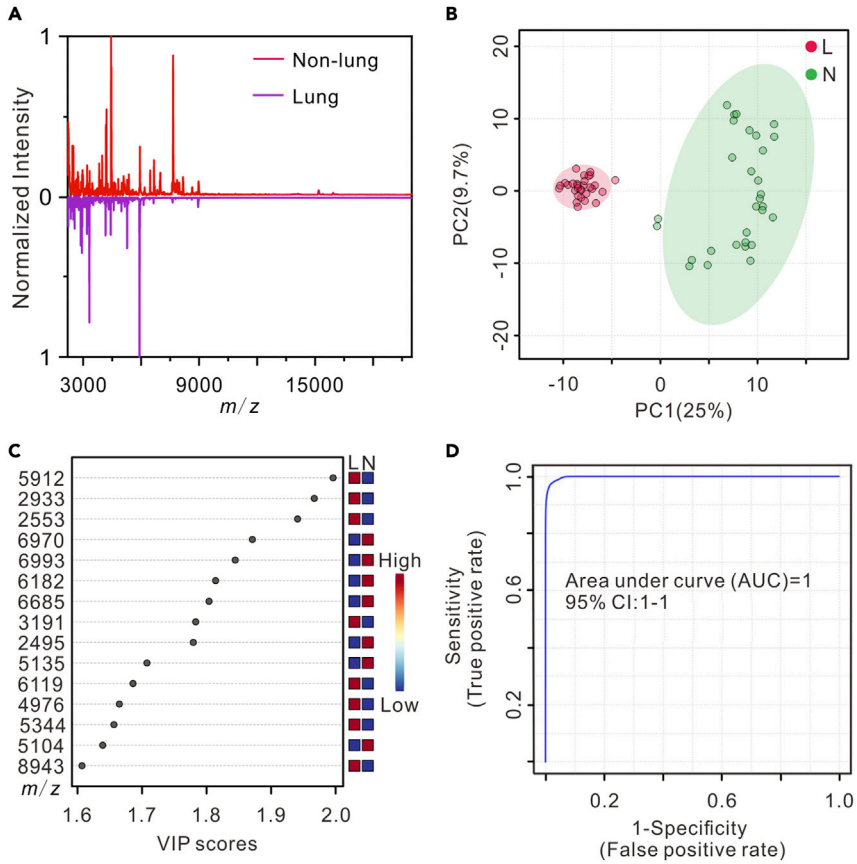

Figure 4. MALDI-TOF mass spectra of plasma-derived exosomes for the identification of osteosarcoma lung metastasis

(A) MALDI-TOF mass spectra of plasma-derived exosomes from a patient with osteosarcoma lung metastasis and a patient with non-lung metastasis.

(B) PCA of the MALDI-TOF data of plasma-derived exosomes from 10 patients with osteosarcoma lung metastasis (L) and 10 patients with non-lung metastasis (N).

(C) Important MALDI-TOF MS features of plasma-derived exosomes from the 10 patients with osteosarcoma lung metastasis (L) compared with the 10 patients with non-lung metastasis (N) identified by PLS-DA.

(D) ROC curve based on 7 significant features (*m/z* = 3266, 3730, 5104, 5135, 5272, 5344, and 7626) plotted by 100-times Monte Carlo cross-validation (MCCV) using MetaboAnalyst 4.0. For MALDI-TOF analyses, three replicates were performed on each sample.

which can be considered as candidate biomarkers. To identify the MALDI-TOF features, proteomic analysis was executed on the pooled plasma-derived exosomes isolated from the patients with osteosarcoma lung metastasis and patients with non-lung metastasis. A total of 353 proteins were identified from the plasma-derived exosomes (Data S2). The MALDI-TOF mass spectra peaks were matched to the proteomic analysis results under the criteria that MALDI-TOF must detect at least two continuous charge states from 1+, 2+, and 3+ of a protein with an *m/z* tolerance of 2000 ppm. Finally, 7 proteins matched with the MALDI-TOF significant features of osteosarcoma lung metastasis selected by the PLS-DA analysis as candidate biomarkers (Table 1), including immunoglobulin lambda variable 2-23 (IGLV2-23), immunoglobulin lambda variable 4-3 (IGLV4-3), immunoglobulin lambda variable 1-51 (IGLV1-51), immunoglobulin kappa variable 3-15 (IGKV3-15), immunoglobulin heavy variable 4-4 (IGHV4-4), immunoglobulin lambda variable 4-60 (IGLV4-60), and hemoglobin subunit alpha (HBA1). To further evaluate the discriminatory power of the 7 potential biomarkers, cross-validation receiver operating characteristic (ROC) analysis was performed. The ROC result showed an area under the curve value of 1.0 (Figure 4D), demonstrating that the 7 proteins can serve as potential biomarkers of osteosarcoma lung metastasis.

Table 1. Seven protein biomarkers of osteosarcoma lung metastasis identified by MALDI-TOF and LC-MS/MS

Feature peak *m/z*	Charge on MALDI-TOF mass spectra	Accession	Molecular weight	Identified protein
3266	3	sp_P01705_LV223_HUMAN	9806	Immunoglobulin lambda variable 2-23 (IGLV2-23)
3730	3	sp_A0A075B6K6_LV403_HUMAN	11,181	Immunoglobulin lambda variable 4-3 (IGLV4-3)
5104	2	sp_P01701_LV151_HUMAN	10,206	Immunoglobulin lambda variable 1-51 (IGLV1-51)
5135	2	sp_P01624_KV315_HUMAN	10,271	Immunoglobulin kappa variable 3-15 (IGKV3-15)
5272	2	sp_A0A075B6R2_HV404_HUMAN	10,537	Immunoglobulin heavy variable 4-4 (IGHV4-4)
5344	2	sp_A0A075B6I1_LV460_HUMAN	10,678	Immunoglobulin lambda variable 4-60 (IGLV4-60)
7626	2	sp_P69905_HBA_HUMAN	15,257	Hemoglobin subunit alpha (HBA1)

To further validate the 7 protein biomarkers for osteosarcoma lung metastasis, another 10 patients with osteosarcoma lung metastasis and 10 patients with non-lung metastasis were recruited as pseudo-blind samples for model test. PCA model was built using the 7 protein biomarkers on the MALDI-TOF data of the training set shown in Figure 4. As shown in Figures 5A and 5B, the test samples were correctly classified, revealing the 7 protein biomarkers robust for the identification of osteosarcoma lung metastasis. The profiling of gene ontology (GO) analysis in Figure 5C showed the biological functions of the 7 protein biomarkers.

DISCUSSION

The predilection age of osteosarcoma is 10–14 years in line with the age of bone growth. The current treatments can achieve a 70% cure rate of patients with osteosarcoma (Kansara et al., 2014). However, metastasis is the leading cause of death of patients with osteosarcoma (Kohama et al., 2019). Metastatic sites of osteosarcoma are detected primarily in the lungs. Therefore, there is an urgent need to develop a robust and straightforward method to diagnose lung metastasis of osteosarcoma, in order to improve the survival of patients with osteosarcoma.

Exosomes are small vesicles with lipid bilayers with the diameter of 30-150 nm, containing nucleic acids, proteins, and lipids (Huang et al., 2020). They are considered to be the means by which cells transmit information, and their delivery cargos can vary greatly depending on the function of the original cell type and its current state (Colombo et al., 2014). It has been reported that exosomes are associated with many human diseases and can serve as surrogate biomarkers for the diagnosis of tumor progression and metastasis instead of invasive clinical procedures (Le et al., 2014). Studies of exosomes relating to osteosarcomas have been performed. Jerez et al. profiled proteins and exosomes derived from three human osteosarcoma cell lines to investigate the intercommunication between osteosarcoma cells and their microenvironment which may promote bone tumor progression and metastasis (Jerez et al., 2017). Wei et al. demonstrated that using exosomes to design nanodrugs can increase cellular uptake efficiency and antitumor effect in osteosarcoma MG63 cell line (Wei et al., 2019). Yan et al. reported that macrophage-derived exosomes can facilitate osteosarcoma progression and drug resistance by activating AKT signaling (Yan et al., 2020). Wang et al. reported that the analysis of exosomal PD-L1 and N-cadherin from the serum of patients with osteosarcoma can monitor lung metastasis progression in patients with osteosarcoma (Wang et al., 2020). The studies on exosomes may lead to a breakthrough in finding an effective osteosarcoma treatment and early diagnosis method.

Despite the studies on exosomes, the profiling of exosomes in clinical samples remains challenging. The currently widely used method for exosomes profiling include ELISA, nano-flow cytometry, and fluorescence imaging based on known protein biomarkers (Cho et al., 2019; Choi et al., 2019). These methods can only

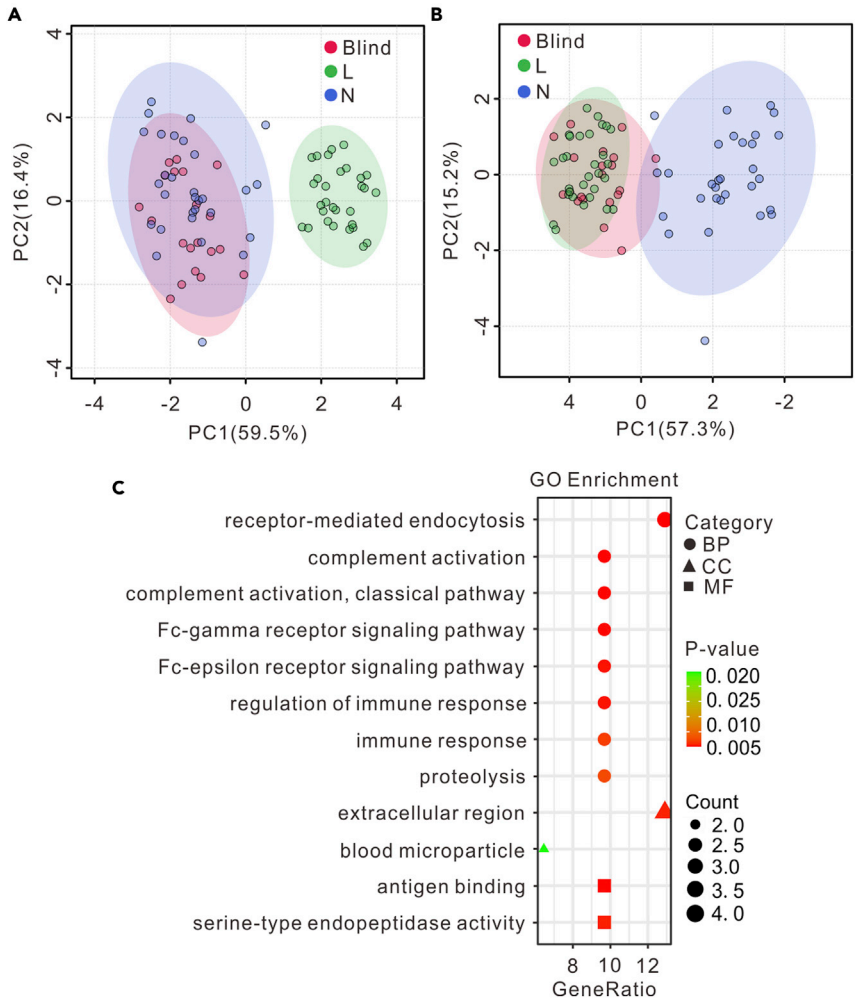

Figure 5. Validation and gene ontology analysis of the 7 protein biomarkers for osteosarcoma lung metastasis

(A and B) Validation of the 7 protein biomarkers using the MALDI-TOF mass fingerprints of plasma-derived exosomes from another (A) 10 patients with non-lung metastasis osteosarcoma (N) and (B) 10 patients with lung metastasis osteosarcoma (L). The PCA model was built with the training data set shown in Figure 4B. For the test data set, two MALDI-TOF replicates were performed on each sample.

(C) Gene ontology enrichment of the 7 protein biomarkers. BP: biological processes; CC: cell component; MF: molecular function.

identify specific subpopulation of exosomes, resulting in the missing information of other extracellular subpopulations, and cannot provide biomolecular composition of the whole exosomes. MALDI-TOF MS is a powerful approach for the profiling of exosomes with advantages in several aspects: 1) label-free for the analysis of exosomal composition; 2) fast detection; and 3) high-throughput analysis. In MALDI-TOF MS analysis, matrix is used to isolate analyte molecules, absorb laser energy, and assist the ionization of analyte molecules. Therefore, it is critical to select an appropriate matrix for MALDI-TOF MS analysis. The commonly used MALDI matrices in protein and peptide analysis include SA, DHB, and HCCA. DHB has strong polarity, generates large crystals, leads to poor uniformity, and is normally used for peptides, glycopeptides, glycoproteins, and proteins (Kaletaş et al., 2009). HCCA and SA matrices can generate small crystals and lead to good homogeneity. HCCA is mainly utilized in polypeptide analysis (Cohen and Chait, 1996; Wiangnon and Cramer, 2015), whereas SA is more suitable for proteins (Marvin et al., 2003). Moreover, it was demonstrated that SA can provide good reproducibility in the detection of biological samples in a wide mass range (Zhu et al., 2018, 2019b), which is in accordance with our results. Hence, SA was chosen in this work for the analysis of exosomes.

We collected the MALDI-TOF mass spectra of plasma-derived exosomes secreted by patients with osteosarcoma with or without lung metastasis, patients with lung cancer, and healthy volunteers. By unsupervised statistical analysis (PCA and hierarchical clustering), it was clear that the mass spectra of plasma-derived exosomes were different between patients with cancer and healthy controls, between patients with different kinds of cancer, and between patients with osteosarcoma with and without lung metastasis. Both males and females were included in the same type of samples, and we did not observe any effect from sex on the results of the study. The significant MALDI-TOF features between the patients with and without lung metastasis were identified by supervised statistical analysis (PLS-DA) and LC-MS/MS-based proteomic analysis. The identified significant features were further validated by using another group of pseudo-blind samples that was independent from the ones used for model training. Seven protein biomarkers were identified for the osteosarcoma lung metastasis, mostly immunoglobulin-related proteins. Immunoglobulins are found at high frequency in plasma-derived exosomes samples and are often associated with various cancer types (Ndede et al., 2019; Shuai et al., 2019; Son et al., 2020; Zhang et al., 2012). It was reported that immunoglobulins in exosomes are closely related to the proliferation, invasion, and cancer metastasis (Jerez et al., 2017). GO analysis in Figure 5C shows that the identified significant proteins participate in the regulation of Fc-gamma receptor signaling pathway and Fc-epsilon receptor signaling pathway, which are involved in the adjustment of the tumor microenvironment (Milane et al., 2015) and are essential to activate immune response to tumor cells. IGLV2-23, IGLV1-51, and IGKV3-15 are components of extracellular exosomes and participate in all the biological processes listed in Figure 5C. IGLV2-23 has been identified in EVs from lung transplant recipients and reported to play a significant role in the transport of small molecules, signal transduction, and extracellular matrix organization (Bansal et al., 2020). IGLV4-3 with increased L-phytohemagglutinin-reactive glycoproteins is involved in the response of breast carcinoma tumor cells to environmental stress (Abbott et al., 2008; Andaluz Aguilar et al., 2020). IGLV1-51 serves as the validating candidate recurrent fusion gene in patients with hepatocellular carcinoma (Zhu et al., 2019a). IGKV3-15 was used for the development of cancer vaccines in B cell non-Hodgkin lymphomas (Martorelli et al., 2012). IGHV4-4 is involved in phagocytosis, innate immune response, and complement activation (Gaudet et al., 2011) and presents in patients with chronic lymphocytic leukemia (CLL) as an unmutated form (Karan-Djurasevic et al., 2012). The exosomal protein, IGLV4-60, participates in antigen binding and is related with immune activation, including immunoglobulin synthesis, programmed cell death, and DNA repair (Bansal et al., 2020). IGLV4-60 is expressed at higher frequency in the cohort of 76 λ^+ CLL cases than that in the 97 λ^+ CLL samples (Widhopf et al., 2008). The exosomal protein, HBA1, is involved in receptor-mediated endocytosis, oxygen transport, positive regulation of cell death, and other biological processes (Keerthikumar et al., 2016; Mathivanan et al., 2012; Mathivanan and Simpson, 2009). HBA1 is utilized for the monitor of glycemic control and can serve as a biomarker in the regulation of prostate cancer (Wu et al., 2020). Furthermore, these proteins in exosomes are related to complement activation with an immune evasion mechanism (Brady et al., 2018) and complement activation within tumor microenvironment to increase tumor growth and disease progression (Gadwa and Karam, 2020). The receptor-mediated endocytosis is beneficial for targeted cancer therapy (Jia et al., 2020). Immune response and its regulation is closely related to cancer development and tumor progression (Becker et al., 2016; Hernandez et al., 2016). Based on the biological roles of the identified significant proteins, the rationality of the biomarkers and the MALDI-TOF-based exosomes profiling method for the detection of osteosarcoma lung metastasis are further demonstrated.

In summary, we show that MALDI-TOF mass fingerprinting of exosomes has great potential in clinical application. The detection and analysis of exosomes will contribute to the diagnosis and intervention of osteosarcoma, thereby being conducive to early prevention. The method can be further applied to find stable biological differences between early cancer metastasis and premetastatic groups, healthy and premetastatic groups, chemotherapy-resistant and nonresistant groups, as well as different subtypes of cancer.

Limitations of the study

Although MALDI-TOF MS profiling of plasma-derived exosomes can distinguish patients with osteosarcoma from healthy controls and distinguish osteosarcoma lung metastasis from non-lung metastasis, the exosomes were collected by ultracentrifugation, which is inefficient and time-consuming. It is preferred to develop efficient methods, e.g., based on microfluidics, for high-throughput purification of exosomes from plasma, and to intergrade the exosomes purification methods with the MALDI-TOF analysis in the follow-up work.

STAR★METHODS

Detailed methods are provided in the online version of this paper and include the following:

- KEY RESOURCES TABLE
- RESOURCE AVAILABILITY
  - Lead contact
  - Materials availability
  - Data and code availability
- EXPERIMENTAL MODEL AND SUBJECT DETAILS
  - Cell culture
  - Human plasma collection
- METHOD DETAILS
  - Isolation of exosomes using ultracentrifugation
  - Characterization of exosomes
  - Western blot
  - MALDI-TOF MS analysis
- QUANTIFICATION AND STATISTICAL ANALYSIS
  - Statistical analysis of MALDI-TOF MS data
  - Protein extraction, digestion, and quantification
  - LC-MS/MS analysis
  - GO enrichment
- ADDITIONAL RESOURCES

SUPPLEMENTAL INFORMATION

Supplemental information can be found online at https://doi.org/10.1016/j.isci.2021.102906.

ACKNOWLEDGMENTS

This work was supported by the National Natural Science Foundation of China (81773298, 21934001, 22022401), Science and Technology Commission of Shanghai Municipality (18441901000, 17411951900), Shanghai Municipal Commission of Health and Family Planning (201740139), and Clinical Research Plan of SHDC (No. SHDC2020CR3078B). We acknowledge Dr. Qiyuan Bao from Ruijin Hospital for his assistance in collecting the clinical samples.

AUTHOR CONTRIBUTIONS

Z.H. performed the experiments and data analysis and wrote the original draft. C.P. performed the experiments. J.Y., Q.L., and Y.Y. helped with the data processing. S.L. collected the clinical samples. L.Q. revised the original draft of the manuscript. Y.W. modified the manuscript. L.Q. and Y.S. acquired the funding for this research and supervised all aspects of the work. All authors were involved in the design of the study. ‡These authors contribute equally to this work.

DECLARATION OF INTERESTS

The authors declare no competing interests.

INCLUSION AND DIVERSITY

We worked to ensure ethnic or other types of diversity in the recruitment of human subjects. We worked to ensure that the study questionnaires were prepared in an inclusive way. The author list of this paper includes contributors from the location where the research was conducted who participated in the data collection, design, analysis, and/or interpretation of the work.

Received: February 9, 2021
Revised: June 8, 2021
Accepted: July 21, 2021
Published: August 20, 2021

REFERENCES

Abbott, K.L., Aoki, K., Lim, J., Porterfield, M., Johnson, R., O'Regan, R.M., Wells, L., Tiemeyer, M., and Pierce, M. (2008). Targeted glycoproteomic identification of biomarkers for human breast carcinoma. J. Proteome Res. *7*, 1470–1480.

Andaluz Aguilar, H., Iliuk, A.B., Chen, I.H., and Tao, W.A. (2020). Sequential phosphoproteomics and N-glycoproteomics of plasma-derived extracellular vesicles. Nat. Protoc. *15*, 161–180.

Bansal, S., McGilvrey, M., Garcia-Mansfield, K., Sharma, R., Bremner, R.M., Smith, M.A., Hachem, R., Pirrotte, P., and Mohanakumar, T. (2020). Global proteomics analysis of circulating extracellular vesicles isolated from lung transplant recipients. ACS Omega *5*, 14360–14369.

Becker, A., Thakur, B.K., Weiss, J.M., Kim, H.S., Peinado, H., and Lyden, D. (2016). Extracellular vesicles in cancer: cell-to-cell mediators of metastasis. Cancer Cell *30*, 836–848.

Behjati, S., Tarpey, P.S., Haase, K., Ye, H., Young, M.D., Alexandrov, L.B., Farndon, S.J., Collord, G., Wedge, D.C., Martincorena, I., et al. (2017). Recurrent mutation of IGF signalling genes and distinct patterns of genomic rearrangement in osteosarcoma. Nat. Commun. *8*, 15936.

Bielack, S.S., Kempf-Bielack, B., Delling, G., Exner, G.U., Flege, S., Flege, S., Helmke, S., Kotz, R., Salzer-Kuntschik, M., Werner, M., et al. (2014). Prognostic factors in high-grade osteosarcoma of the extremities or trunk: an analysis of 1,702 patients treated on neoadjuvant cooperative osteosarcoma study group protocols. J. Clin. Oncol. *20*, 776–790.

Brady, J.V., Troyer, R.M., Ramsey, S.A., Leeper, H., Yang, L., Maier, C.S., Goodall, C.P., Ruby, C.E., Albarqi, H.A.M., Taratula, O., et al. (2018). A preliminary proteomic investigation of circulating exosomes and discovery of biomarkers associated with the progression of osteosarcoma in a clinical model of spontaneous disease. Transl. Oncol. *11*, 1137–1146.

Brock, G., Castellanos-Rizaldos, E., Hu, L., Coticchia, C., and Skog, J. (2015). Liquid biopsy for cancer screening, patient stratification and monitoring. Transl. Cancer Res. *4*, 280–290.

Butts, C.A. (2014). VeriStrat validated in patients with non-small-cell lung cancer. Lancet Oncol. *15*, 671–672.

Chen, G., Huang, A.C., Zhang, W., Zhang, G., Wu, M., Xu, W., Yu, Z., Yang, J., Wang, B., Sun, H., et al. (2018). Exosomal PD-L1 contributes to immunosuppression and is associated with anti-PD-1 response. Nature *560*, 382–386.

Chicon-Bosch, M., and Tirado, O.M. (2020). Exosomes in bone sarcomas: key players in metastasis. Cells *9*, 241.

Cho, S., Yang, H.C., and Rhee, W.J. (2019). Simultaneous multiplexed detection of exosomal microRNAs and surface proteins for prostate cancer diagnosis. Biosens. Bioelectron. *146*, 111749.

Choi, D., Montermini, L., Jeong, H., Sharma, S., Meehan, B., and Rak, J. (2019). Mapping subpopulations of cancer cell-derived extracellular vesicles and particles by nano-flow cytometry. ACS Nano *13*, 10499–10511.

Chong, J., Soufan, O., Li, C., Caraus, I., Li, S., Bourque, G., Wishart, D.S., and Xia, J. (2018). MetaboAnalyst 4.0: towards more transparent and integrative metabolomics analysis. Nucleic Acids Res. *46*, W486–W494.

Cohen, S.L., and Chait, B.T. (1996). Influence of matrix solution conditions on the MALDI-MS analysis of peptides and proteins. Anal. Chem. *68*, 31–37.

Colombo, M., Raposo, G., and Thery, C. (2014). Biogenesis, secretion, and intercellular interactions of exosomes and other extracellular vesicles. Annu. Rev. Cell Dev. Biol. *30*, 255–289.

Costa-Silva, B., Aiello, N.M., Ocean, A.J., Singh, S., Zhang, H., Thakur, B.K., Becker, A., Hoshino, A., Mark, M.T., Molina, H., et al. (2015). Pancreatic cancer exosomes initiate pre-metastatic niche formation in the liver. Nat. Cell Biol. *17*, 816–826.

Deutsch, E.W., Bandeira, N., Sharma, V., Perez-Riverol, Y., Carver, J.J., Kundu, D.J., Garcia-Seisdedos, D., Jarnuczak, A.F., Hewapathirana, S., Pullman, B.S., et al. (2020). The ProteomeXchange consortium in 2020: enabling 'big data' approaches in proteomics. Nucleic Acids Res. *48*, D1145–D1152.

Di, H., Zeng, E., Zhang, P., Liu, X., Zhang, C., Yang, J., and Liu, D. (2019). General approach to engineering extracellular vesicles for biomedical analysis. Anal. Chem. *91*, 12752–12759.

Gadwa, J., and Karam, S.D. (2020). Deciphering the intricate roles of radiation therapy and complement activation in cancer. Int. J. Radiat. Oncol. Biol. Phys. *108*, 46–55.

Galardi, A., Colletti, M., Di Paolo, V., Vitullo, P., Antonetti, L., Russo, I., and Di Giannatale, A. (2019). Exosomal miRNAs in pediatric cancers. Int. J. Mol. Sci. *20*, 4600.

Gardiner, C., Ferreira, Y.J., Dragovic, R.A., Redman, C.W., and Sargent, I.L. (2013). Extracellular vesicle sizing and enumeration by nanoparticle tracking analysis. J. Extracell. Vesicles *2*, 19671.

Gaudet, P., Livstone, M.S., Lewis, S.E., and Thomas, P.D. (2011). Phylogenetic-based propagation of functional annotations within the Gene Ontology consortium. Brief. Bioinform. *12*, 449–462.

Gerlinger, M., Rowan, A.J., Horswell, S., Math, M., Larkin, J., Endesfelder, D., Gronroos, E., Martinez, P., Matthews, N., Stewart, A., et al. (2012). Intratumor heterogeneity and branched evolution revealed by multiregion sequencing. N. Engl. J. Med. *366*, 883–892.

Gibb, S., and Strimmer, K. (2012). MALDIquant: a versatile R package for the analysis of mass spectrometry data. Bioinformatics *28*, 2270–2271.

Hernandez, C., Huebener, P., and Schwabe, R.F. (2016). Damage-associated molecular patterns in cancer: a double-edged sword. Oncogene *35*, 5931–5941.

Hoshino, A., Kim, H.S., Bojmar, L., Gyan, K.E., Cioffi, M., Hernandez, J., Zambirinis, C.P., Rodrigues, G., Molina, H., Heissel, S., et al. (2020). Extracellular vesicle and particle biomarkers define multiple human cancers. Cell *182*, 1–18.

Huang da, W., Sherman, B.T., and Lempicki, R.A. (2009). Systematic and integrative analysis of large gene lists using DAVID bioinformatics resources. Nat. Protoc. *4*, 44–57.

Huang, G., Lin, G., Zhu, Y., Duan, W., and Jin, D. (2020). Emerging technologies for profiling extracellular vesicle heterogeneity. Lab Chip *20*, 2423–2437.

Jagadeesan, K.K., and Ekstrom, S. (2017). MALDIViz: a comprehensive informatics tool for MALDI-MS data visualization and analysis. SLAS Discov. *22*, 1246–1252.

Jansen, F.H., Krijgsveld, J., van Rijswijk, A., van den Bemd, G.J., van den Berg, M.S., van Weerden, W.M., Willemsen, R., Dekker, L.J., Luider, T.M., and Jenster, G. (2009). Exosomal secretion of cytoplasmic prostate cancer xenograft-derived proteins. Mol. Cell. Proteomics *8*, 1192–1205.

Jerez, S., Araya, H., Thaler, R., Charlesworth, M.C., Lopez-Solis, R., Kalergis, A.M., Cespedes, P.F., Dudakovic, A., Stein, G.S., van Wijnen, A.J., et al. (2017). Proteomic analysis of exosomes and exosome-free conditioned media from human osteosarcoma cell lines reveals secretion of proteins related to tumor progression. J. Cell. Biochem. *118*, 351–360.

Jia, X., Xu, W., Ye, Z., Wang, Y., Dong, Q., Wang, E., Li, D., and Wang, J. (2020). Functionalized graphene@gold nanostar/lipid for pancreatic cancer gene and photothermal synergistic therapy under photoacoustic/photothermal imaging dual-modal guidance. Small *16*, e2003707.

Kaletaş, B.K., van der Wiel, I.M., Stauber, J., Dekker, L.J., Güzel, C., Kros, J.M., Luider, T.M., and Heeren, R.M.A. (2009). Sample preparation issues for tissue imaging by imaging MS. Proteomics *9*, 2622–2633.

Kansara, M., Teng, M.W., Smyth, M.J., and Thomas, D.M. (2014). Translational biology of osteosarcoma. Nat. Rev. Cancer *14*, 722–735.

Karan-Djurasevic, T., Palibrk, V., Kostic, T., Spasovski, V., Nikcevic, G., Srzentic, S., Colovic, M., Colovic, N., Vidovic, A., Antic, D., et al. (2012). Mutational status and gene repertoire of IGHV-IGHD-IGHJ rearrangements in Serbian patients with chronic lymphocytic leukemia. Clin. Lymphoma Myeloma Leuk. *12*, 252–260.

Keerthikumar, S., Chisanga, D., Ariyaratne, D., Al Saffar, H., Anand, S., Zhao, K., Samuel, M., Pathan, M., Jois, M., Chilamkurti, N., et al. (2016). ExoCarta: a web-based compendium of exosomal cargo. J. Mol. Biol. *428*, 688–692.

Keklikoglou, I., Cianciaruso, C., Guc, E., Squadrito, M.L., Spring, L.M., Tazzyman, S., Lambein, L., Poissonnier, A., Ferraro, G.B., Baer, C., et al. (2019). Chemotherapy elicits pro-metastatic extracellular vesicles in breast cancer models. Nat. Cell Biol. *21*, 190–202.

Kohama, I., Kosaka, N., Chikuda, H., and Ochiya, T. (2019). An insight into the roles of microRNAs and exosomes in sarcoma. Cancers *11*, 428.

Le, M.T., Hamar, P., Guo, C., Basar, E., Perdigao-Henriques, R., Balaj, L., and Lieberman, J. (2014). MiR-200-containing extracellular vesicles promote breast cancer cell metastasis. J. Clin. Invest. *124*, 5109–5128.

Lin, S.Y., Chang, C.H., Wu, H.C., Lin, C.C., Chang, K.P., Yang, C.R., Huang, C.P., Hsu, W.H., Chang, C.T., and Chen, C.J. (2016). Proteome profiling of urinary exosomes identifies Alpha 1-antitrypsin and H2B1K as diagnostic and prognostic biomarkers for urothelial carcinoma. Sci. Rep. *6*, 34446.

Liu, C., Zhao, Z., Fan, J., Lyon, C.J., Wu, H.J., Nedelkov, D., Zelazny, A.M., Olivier, K.N., Cazares, L.H., Holland, S.M., et al. (2017). Quantification of circulating Mycobacterium tuberculosis antigen peptides allows rapid diagnosis of active disease and treatment monitoring. Proc. Natl. Acad. Sci. U S A *114*, 3969–3974.

Liu, K., Gao, L., Ma, X., Huang, J.J., Chen, J., Zeng, L., Ashby, C.R., Zou, C., and Chen, Z.S. (2020). Long non-coding RNAs regulate drug resistance in cancer. Mol. Cancer *19*, 54.

Luetke, A., Meyers, P.A., Lewis, I., and Juergens, H. (2014). Osteosarcoma treatment - where do we stand? A state of the art review. Cancer Treat. Rev. *40*, 523–532.

Martorelli, D., Guidoboni, M., De Re, V., Muraro, E., Turrini, R., Merlo, A., Pasini, E., Caggiari, L., Romagnoli, L., Spina, M., et al. (2012). IGKV3 proteins as candidate "off-the-shelf" vaccines for kappa-light chain-restricted B-cell non-Hodgkin lymphomas. Clin. Cancer Res. *18*, 4080–4091.

Marvin, L.F., Roberts, M.A., and Fay, L.B. (2003). Matrix-assisted laser desorption/ionization time-of-flight mass spectrometry in clinical chemistry. Clin. Chim. Acta *337*, 11–21.

Mathivanan, S., Fahner, C.J., Reid, G.E., and Simpson, R.J. (2012). ExoCarta 2012: database of exosomal proteins, RNA and lipids. Nucleic Acids Res. *40*, D1241–D1244.

Mathivanan, S., and Simpson, R.J. (2009). ExoCarta: a compendium of exosomal proteins and RNA. Proteomics *9*, 4997–5000.

Meyers, P.A., Healey, J.H., Chou, A.J., Wexler, L.H., Merola, P.R., Morris, C.D., Laquaglia, M.P., Kellick, M.G., Abramson, S.J., and Gorlick, R. (2011). Addition of pamidronate to chemotherapy for the treatment of osteosarcoma. Cancer *117*, 1736–1744.

Milane, L., Singh, A., Mattheolabakis, G., Suresh, M., and Amiji, M.M. (2015). Exosome mediated communication within the tumor microenvironment. J. Control Release *219*, 278–294.

Morhayim, J., van de Peppel, J., Dudakovic, A., Chiba, H., van Wijnen, A.J., and van Leeuwen, J.P. (2017). Molecular characterization of human osteoblast-derived extracellular vesicle mRNA using next-generation sequencing. Biochim. Biophys. Acta Mol. Cell Res. *1864*, 1133–1141.

Nakamura, A., Kaneko, N., Villemagne, V.L., Kato, T., Doecke, J., Dore, V., Fowler, C., Li, Q.X., Martins, R., Rowe, C., et al. (2018). High performance plasma amyloid-beta biomarkers for Alzheimer's disease. Nature *554*, 249–254.

Ndede, I., Mining, S.K., Patel, K., Wanjala, F.M., and Tenge, C. (2019). Immunoglobulin heavy variable (IgHV) gene mutation and micro-RNA expression in Burkitt's lymphoma at Moi Teaching and Referral Hospital in Western Kenya. Afr. Health Sci. *19*, 3242–3248.

Nguyen, H.-Q., Lee, D., Kim, Y., Paek, M., Kim, M., Jang, K.-S., Oh, J., Lee, Y.-S., Yeon, J.E., Lubman, D.M., et al. (2019). Platelet factor 4 as a novel exosome marker in MALDI-MS analysis of exosomes from human serum. Anal. Chem. *91*, 13297–13305.

Palmieri, V., Lucchetti, D., Gatto, I., Maiorana, A., Marcantoni, M., Maulucci, G., Papi, M., Pola, R., De Spirito, M., and Sgambato, A. (2014). Dynamic light scattering for the characterization and counting of extracellular vesicles: a powerful noninvasive tool. J. Nanopart. Res. *16*, 2583.

Perez-Riverol, Y., Csordas, A., Bai, J., Bernal-Llinares, M., Hewapathirana, S., Kundu, D.J., Inuganti, A., Griss, J., Mayer, G., Eisenacher, M., et al. (2019). The PRIDE database and related tools and resources in 2019: improving support for quantification data. Nucleic Acids Res. *47*, D442–D450.

Perez-Riverol, Y., Xu, Q.W., Wang, R., Uszkoreit, J., Griss, J., Sanchez, A., Reisinger, F., Csordas, A., Ternent, T., Del-Toro, N., et al. (2016). PRIDE inspector toolsuite: moving toward a universal visualization tool for proteomics data standard formats and quality assessment of ProteomeXchange datasets. Mol. Cell. Proteomics *15*, 305–317.

Rat, A., Glibowick, M., Nadeau, V.G., Chen, C., and Deber, C.M. (2008). Detergent binding explains anomalous SDS-PAGE migration of membrane proteins. Proc. Natl. Acad. Sci. U S A *106*, 1760–1765.

Rathore, R., Corr, J., Scott, G., Vollmerhaus, P., and Greis, K.D. (2008). Development of an inhibitor screening platform via mass spectrometry. J. Biomol. Screen. *13*, 1007–1013.

Saenz-Pipaon, G., San Martin, P., Planell, N., Maillo, A., Ravassa, S., Vilas-Zornoza, A., Martinez-Aguilar, E., Rodriguez, J.A., Alameda, D., Lara-Astiaso, D., et al. (2020). Functional and transcriptomic analysis of extracellular vesicles identifies calprotectin as a new prognostic marker in peripheral arterial disease (PAD). J. Extracell. Vesicles *9*, 1729646.

Shuai, S., Suzuki, H., Diaz-Navarro, A., Nadeu, F., Kumar, S.A., Gutierrez-Fernandez, A., Delgado, J., Pinyol, M., Lopez-Otin, C., Puente, X.S., et al. (2019). The U1 spliceosomal RNA is recurrently mutated in multiple cancers. Nature *574*, 712–716.

Singhto, N., Vinaiphat, A., and Thongboonkerd, V. (2019). Discrimination of urinary exosomes from microvesicles by lipidomics using thin layer liquid chromatography (TLC) coupled with MALDI-TOF mass spectrometry. Sci. Rep. *9*, 13834.

Son, K.H., Ahn, C.B., Kim, H.J., and Kim, J.S. (2020). Quantitative proteomic analysis of bile in extrahepatic cholangiocarcinoma patients. J. Cancer *11*, 4073–4080.

Stübiger, G., Nairn, M.D., Abban, T.K., Openshaw, M.E., Mancera, L., Herzig, B., Wuczkowski, M., Senfter, D., and Mader, R.M. (2018). MALDI-MS protein profiling of chemoresistance in extracellular vesicles of cancer cells. Anal. Chem. *90*, 13178–13182.

Thery, C., Clayton, A., Amigorena, S., and Raposo, G. (2006). Isolation and characterization of exosomes from cell culture supernatants and biological fluids. Curr. Protoc. Cell Biol. *3*, 3.22.

Tieu, A., Lalu, M.M., Slobodian, M., Gnyra, C., Fergusson, D.A., Montroy, J., Burger, D., Stewart, D.J., and Allan, D.S. (2020). An analysis of mesenchymal stem cell-derived extracellular vesicles for preclinical use. ACS Nano *14*, 9728–9743.

Varadi, L., Luo, J.L., Hibbs, D.E., Perry, J.D., Anderson, R.J., Orenga, S., and Groundwater, P.W. (2017). Methods for the detection and identification of pathogenic bacteria: past, present, and future. Chem. Soc. Rev. *46*, 4818–4832.

Vogel, R., Coumans, F.A.W., Maltesen, R.G., Boing, A.N., Bonnington, K.E., Broekman, M.L., Broom, M.F., Buzas, E.I., Christiansen, G., Hajji, N., et al. (2016). A standardized method to determine the concentration of extracellular vesicles using tunable resistive pulse sensing. J. Extracell. Vesicles *5*, 31242.

Wang, J., Zhang, H., Sun, X., Wang, X., Ren, T., Huang, Y., Zhang, R., Zheng, B., and Guo, W. (2020). Exosomal PD-L1 and N-cadherin predict pulmonary metastasis progression for osteosarcoma patients. J. Nanobiotechnology *18*, 151.

Wei, H., Chen, J., Wang, S., Fu, F., Zhu, X., Wu, C., Liu, Z., Zhong, G., and Lin, J. (2019). A nanodrug consisting of doxorubicin and exosome derived from mesenchymal stem cells for osteosarcoma treatment in vitro. Int. J. Nanomedicine *14*, 8603–8610.

Welsh, J.A., Van Der Pol, E., Arkesteijn, G.J.A., Bremer, M., Brisson, A., Coumans, F., Dignat-George, F., Duggan, E., Ghiran, I., Giebel, B., et al. (2020). MIFlowCyt-EV: a framework for standardized reporting of extracellular vesicle flow cytometry experiments. J. Extracell. Vesicles *9*, 1713526.

Wiangnon, K., and Cramer, R. (2015). Sample preparation: a crucial factor for the analytical performance of rationally designed MALDI matrices. Anal. Chem. *87*, 1485–1488.

Widhopf, G.F., Goldberg, C.J., Toy, T.L., Rassenti, L.Z., Wierda, W.G., Byrd, J.C., Keating, M.J., Gribben, J.G., Rai, K.R., and Kipps, T.J. (2008). Nonstochastic pairing of immunoglobulin heavy and light chains expressed by chronic lymphocytic leukemia B cells is predicated on the heavy chain CDR3. Blood *111*, 3137–3144.

Witwer, K.W., Buzas, E.I., Bemis, L.T., Bora, A., Lasser, C., Lotvall, J., Nolte-'t Hoen, E.N., Piper, M.G., Sivaraman, S., Skog, J., et al. (2013). Standardization of sample collection, isolation

and analysis methods in extracellular vesicle research. J. Extracell. Vesicles *2*, 20360.

Wu, Y.P., Ke, Z.B., Lin, F., Wen, Y.A., Chen, S., Li, X.D., Chen, S.H., Sun, X.L., Huang, J.B., Zheng, Q.S., et al. (2020). Identification of key genes and pathways in castrate-resistant prostate cancer by integrated bioinformatics analysis. Pathol. Res. Pract. *216*, 153109.

Yan, B., Liu, Q., Liu, G., Huang, X., Zhu, G., Gao, L., and Xu, Y. (2020). Macrophage-derived exosomes mediate osteosarcoma cell behavior by activating AKT signaling. RSC Adv. *10*, 5032–5039.

Yan, L., Yi, J., Huang, C., Zhang, J., Fu, S., Li, Z., Lyu, Q., Xu, Y., Wang, K., Yang, H., et al. (2021). Rapid detection of COVID-19 using MALDI-TOF-based serum peptidome profiling. Anal. Chem. *93*, 4782–4787.

Yang, J., Hagen, J., Guntur, K.V., Allette, K., Schuyler, S., Ranjan, J., Petralia, F., Gesta, S., Sebra, R., Mahajan, M., et al. (2017a). A next generation sequencing based approach to identify extracellular vesicle mediated mRNA transfers between cells. BMC Genomics *18*, 987.

Yang, Y., Lin, Y., Chen, Z., Gong, T., Yang, P., Girault, H., Liu, B., and Qiao, L. (2017b). Bacterial whole cell typing by mass spectra pattern matching with bootstrapping assessment. Anal. Chem. *89*, 12556–12561.

Yang, Y., Zhai, C., Zeng, Q., Khan, A.L., and Yu, H. (2020). Multifunctional detection of extracellular vesicles with surface plasmon resonance microscopy. Anal. Chem. *92*, 4884–4890.

Yi, J., Qin, Q., Wang, Y., Zhang, R., Bi, H., Yu, S., Liu, B., and Qiao, L. (2018). Identification of pathogenic bacteria in human blood using IgG-modified Fe_3O_4 magnetic beads as a sorbent and MALDI-TOF MS for profiling. Mikrochim. Acta *185*, 542.

Yi, J., Wang, X., Dai, Y., Qiao, L., and Liu, B. (2019). Plasmonic colloidosome-based multifunctional platform for bacterial identification and antimicrobial resistance detection. Anal. Chem. *91*, 14220–14225.

Zhang, L., Hu, S., Korteweg, C., Chen, Z., Qiu, Y., Su, M., and Gu, J. (2012). Expression of immunoglobulin G in esophageal squamous cell carcinomas and its association with tumor grade and Ki67. Hum. Pathol. *43*, 423–434.

Zhu, Y., Gasilova, N., Jovic, M., Qiao, L., Liu, B., Lovey, L.T., Pick, H., and Girault, H.H. (2018). Detection of antimicrobial resistance-associated proteins by titanium dioxide-facilitated intact bacteria mass spectrometry. Chem. Sci. *9*, 2212–2221.

Zhu, C., Wu, L., Lv, Y., Guan, J., Bai, X., Lin, J., Liu, T., Yang, X., Robson, S.C., Sang, X., et al. (2019a). The fusion landscape of hepatocellular carcinoma. Mol. Oncol. *13*, 1214–1225.

Zhu, Y., Pick, H., Gasilova, N., Li, X., Lin, T.-E., Laeubli, H.P., Zippelius, A., Ho, P.-C., and Girault, H.H. (2019b). MALDI detection of exosomes: a potential tool for cancer studies. Chem *5*, 1318–1336.

STAR★METHODS

KEY RESOURCES TABLE

REAGENT or RESOURCE	SOURCE	IDENTIFIER
Antibodies		
Mouse monoclonal anti-CD9	Abcam	Cat# ab2215; RRID: AB_302894
Mouse monoclonal anti-CD81	Abcam	Cat# ab59477; RRID: AB_943630
Mouse monoclonal anti-CD63	Abcam	Cat# ab59479; RRID: AB_940915
Rabbit monoclonal anti-Calnexin	Abcam	Cat# 2692-1; RRID: AB_2259493
Rabbit polyclonal anti-TSG101	Absin	Vat# abs137904
Biological samples		
Human plasma	Ruijin Hospital, Shanghai Jiao Tong University School of Medicine	ClinicalTrials.gov (trial ID: NCT03108677);
Chemicals, peptides, and recombinant proteins		
Cytochrome C	Sigma-Aldrich	C2506; CAS: 9007-43-6
Myoglobin	Sigma-Aldrich	M0632; CAS: 100684-32-0
Sinapic acid	Sigma-Aldrich	85429; CAS: 530-59-6
α-Cyano-4-hydroxycinnamic acid	Sigma-Aldrich	70990; CAS: 28166-41-8
2,5-Dihydroxybenzoic acid	Sigma-Aldrich	149357; CAS: 490-79-9
Phosphotungstic acid	Adamas	17191B; CAS: 12067-99-1
Trifluoroacetic acid	Adamas	B81548A; CAS: 76-05-1
Acetonitrile	Merck	1.00030.4000; CAS: 75-05-8
Deposited data		
Raw proteome data	This manuscript; ProteomeXchange; Mendeley Data;	PXD024072; https://doi.org/10.17632/r5snnfc89s.1
Experimental models: Cell lines		
Human: 143B cell line	ATCC	CRL-8303
Human: HOS cell line	ATCC	CRL-1543
Human: MG63 cell line	ATCC	CRL-1427
Human: U2OS cell line	ATCC	HTP-96
Mouse: 3T3E1 cell line	ATCC	CRL-2593
Software and algorithms		
Origin software	OriginLab	https://www.originlab.com/
Metaboanalyst 4.0	McGill University, Montreal, Canada	https://www.metaboanalyst.ca/
CorelDraw Graphics Suite software	Corel, Ottawa, Canada	https://www.coreldraw.com/en/product/coreldraw/
Flexanalysis	Bruker, Bremen, Germany	NA
Other		
DMEM	Gibco	Cat# 11995065
FBS	Gibco	Cat# 10099141
Penicillin-streptomycin	Gibco	Cat# 15140-122
PBS	HyClone	Cat# SH30256.01
Trypsin	Gibco	Cat# 25200056
MEM Alpha	Gibco	Cat# 12641800

RESOURCE AVAILABILITY

Lead contact

Further information and requests for resources should be directed to and will be fulfilled by the lead contact, Liang Qiao (liang_qiao@fudan.edu.cn).

Materials availability

All reagents generated in this study are available without restriction. This study did not generate new unique reagents.

Data and code availability

The data of this study are available within the article and supplementary information. The peak intensity matrix of all the samples is listed in Sheet AlignmentMatrix (Data S1), which is derived from the raw MALDI-TOF data after data preprocessing and peak alignment by MALDIquant. Machine learning data are listed in Sheet Osteosarcoma Discrimination, Sheet Osteosarcoma Specificity, Sheet TrainingCohort, and Sheet TestCohort (Data S1), which are derived from Sheet AlignmentMatrix after log2 transformation and quantile normalization.

The raw proteome data have been deposited to ProteomeXchange via the PRIDE (Deutsch et al., 2020; Perez-Riverol et al., 2016, 2019) partner repository with the data set identifier PXD024072 and Mendeley Data (https://doi.org/10.17632/r5snnfc89s.1), which are publicly available. Accession numbers are listed in the key resources table.

There is no original code reported in this work.

Any additional information required to reanalyze the data reported in this paper is available from the lead contact upon request.

EXPERIMENTAL MODEL AND SUBJECT DETAILS

Cell culture

The high aggressive osteosarcoma cell lines (143B and HOS cells) (ATCC, Manassas, VA) and low-invasive osteosarcoma cell lines (MG63 and U2OS cells) (ATCC, Manassas, VA) were cultured in Dulbecco's modified eagle medium (DMEM) with 10% EV-depleted fetal bovine serum (FBS) and 1% penicillin-streptomycin at 37°C in a humid atmosphere with 5% CO_2. When the cells reached 40% confluency (Keklikoglou et al., 2019), they were washed twice by 0.01 M phosphate buffered saline (PBS) and then cultured for 24 h in the DMEM with 10% exosomes-depleted FBS and 1% penicillin-streptomycin to reach a confluency of 80%-90%. The normal osteoblast cells, 3T3E1 cells (ATCC, Manassas, VA), were cultured by the same method except that DMEM was replaced by MEM Alpha. The thawed FBS was ultracentrifuged at 120,000 *g* for 14 h and then filtered with a 0.22-um filter to obtain the exosomes-depleted FBS.

Human plasma collection

Forty patients with osteosarcoma with (n = 20) or without (n = 20) lung metastasis and 5 patients with lung cancer as well as 12 heathy controls were randomly recruited from our longitudinal observational clinical research project. Twenty patients with osteosarcoma lung metastasis consisted of 14 males aged 13–62 years and 6 females aged 13–46 years. Twenty patients with osteosarcoma non-lung metastasis consisted of 13 males aged 5–38 years and 7 females aged 11–69 years. Five patients with lung cancer consisted of 4 males aged 51–67 years and 1 female aged 60 years. Twelve healthy controls consisted of 8 males aged 10–57 years and 4 females aged 30–39 years. The detailed gender, age, and developmental stage of subjects can be found in Table S2. Five milliliters of fresh blood was collected from each of subjects. Blood samples collected in disposable vacuum blood vessel collection tubes were kept for 10 min at room temperature, followed by centrifugation at 2000 *g* for 10 min and 3500 *g* for 10 min to eliminate cells and debris. Finally, the plasma samples were collected and stored at −80°C for further usage.

METHOD DETAILS

Isolation of exosomes using ultracentrifugation

Exosomes were isolated from cell culture supernatant using the ultracentrifugation method (Thery et al., 2006). Briefly, 45 mL of culture medium was centrifuged at 500 *g* for 5 min, 2000 *g* for 15 min, and 10,000 *g* for 30 min under 4°C and then filtered through a 0.45-μm filter to remove dead cells, debris, and microvesicles. Subsequently, the supernatant was ultracentrifuged at 110,000 *g* for 11 h, and then the pellets were resuspended in 1×PBS followed by ultracentrifugation at 110,000 *g* for 90 min under 4°C. Finally, the collected exosomes were resuspended in 100 μL of deionized (DI) water and kept under −80°C. To isolate exosomes from plasma sample, 8 mL of 8× diluted plasma by PBS was centrifuged at 10,000 *g* for 30 min and then processed by ultracentrifugation at 110,000 *g* twice as described earlier. The collected plasma-derived exosomes were resuspended in 100 μL of DI water.

Characterization of exosomes

Size and morphology of the collected exosomes were characterized using a JEM 2011 transmission electron microscope (JEOL, Tokyo, Japan). Twenty microliters of exosome pellets were loaded on a 200-mesh carbon-coated copper grid, negatively stained with 2% phosphotungstic acid for 10 min, dried under an infrared lamp, and then observed under a working voltage of 200 kV. Exosomes were also analyzed using a ZetaView® BASIC Nanoparticle Tracking Video Microscope PMX-120 (Particle Metrix, Meerbusch, Germany) for size distribution and concentration characterization.

Western blot

Exosomes were lysed by radioimmunoprecipitation assay (RIPA) protein lysis buffer (EpiZyme, Cambridge, UK). The protein concentration of exosomes was determined by using a bicinchoninic acid (BCA) protein assay kit (Beyotime, Shanghai, China). Total proteins (30 μg) were loaded and separated on 10% sodium dodecyl sulfate polyacrylamide gel electrophores (SDS-PAGE) Bis-Tris Gels (Biotech Well, Hong Kong, China) and then transferred to a 0.45-μm polyvinylidene fluoride (PVDF) membrane (Millipore, Bedford, USA). The membrane was blocked with blotting-grade blocker nonfat dry milk in tris buffered saline Tween (1× TBST, tris 10 mM, NaCl 150 mM, Tween-20 0.05%, pH 7.6) for 1 h and then washed three times with TBST. Subsequently, the primary antibodies, mouse anti-CD63 antibody (1:250; Abcam, Cambridge, UK), mouse anti-CD81 antibody (1:250; Abcam, Cambridge, UK), mouse anti-CD9 antibody (1:250; Abcam, Cambridge, UK), rabbit anti-TSG101 antibody (1:1000; Absin, Shanghai, China), and mouse anti-Calnexin antibody (1:200; Abcam, Cambridge, UK) were used and incubated with membrane overnight at 4°C. To investigate the expression of CD63, CD81, CD9, TSG101, and Calnexin, the separation was performed under nonreducing conditions. For the other proteins, the separation was performed under reducing conditions. Then, the corresponding secondary horseradish peroxidase (HRP) conjugated antibodies were used to incubate with the membrane, and then the immunoreactive bands were detected with a chemiluminescent substrate (ECL TransGen Biotech, Beijing, China). Finally, the scanning images were analyzed using Image J software.

MALDI-TOF MS analysis

MALDI-TOF analysis was performed on a Microflex LRF MALDI-TOF mass spectrometer (Bruker, Bremen, Germany) equipped with a pulsed 337-nm nitrogen laser using SA (20 mg/mL in 50% acetonitrile [ACN]/50% water/0.1% TFA v/v/v), HCCA (10 mg/mL in 30% ACN/70% water/0.1% TFA v/v/v), and DHB (10 mg/mL in 30% ACN/70% water/0.1% TFA v/v/v) matrix. One microliter of sample was deposited on a Microflex Anchorchip plate (Bruker, Bremen, Germany), dried under ambient condition, and then overlayered with 1 μL of matrix. When the matrix was dried, MALDI-TOF MS analysis was performed under linear positive mode. The optimized parameters were as follows: 70% laser intensity, laser attenuator with 35% offset and 40% range, accumulation of 500 laser shots, 10.3× detector gain, and 150 ns delayed extraction time. External mass calibration was performed using cytochrome c (2 mg/mL) and myoglobin (2 mg/mL).

QUANTIFICATION AND STATISTICAL ANALYSIS

Statistical analysis of MALDI-TOF MS data

Raw data obtained from MALDI-TOF MS were converted to txt format with Flexanalysis (Bruker, Bremen, Germany) and then processed using the R packages MALDIquant and MALDIquantForeign (http://www.strimmerlab.org/software/maldiquant/) (Gibb and Strimmer, 2012). Briefly, the mass range was set to 2 to 20 kDa. Then, the square root transformation was performed, followed by Savitzky-Golay smoothing

and statistics-sensitive nonlinear iterative peak-clipping (SNIP) baseline correction. The warpMassSpectra command was performed for the mass value alignment. The signal-to-noise ratio of peak detection was set to 3, and the half window size was set to 20. Peaks were removed with the binPeaks command with a tolerance of 0.002. Finally, a peak intensity matrix was obtained including the *m/z* values and intensity of peaks normalized by the sum intensity of the corresponding mass spectrum. Multivariate statistical analyses, including data transformation (log2 transformation and autoscaling), PCA, PLS-DA, hierarchical clustering, and multivariate ROC curve analysis, were performed on the obtained peak intensity matrix using Metaboanalyst 4.0 (McGill University, Montreal, Canada, https://www.metaboanalyst.ca/) (Chong et al., 2018) and BacteriaMS (Fudan University, Shanghai, China, http://bacteriams.com/) (Yang et al., 2017b). Briefly, the statistical analysis was performed on the MetaboAnalyst 4.0 web server, where the peak intensity matrix was uploaded, followed by normalization by sum, log2 transformation, and autoscaling. Then, analysis paths, such as PCA, PLS-DA, *etc*, were chosen to explore the results. Finally, the figures of multivariate statistical analyses can be directly obtained using Metaboanalyst 4.0 analysis, and other figures of mass spectra were plotted by Origin software (OriginLab, Northampton, MA, USA). CorelDraw Graphics Suite software (Corel, Ottawa, Canada) was used for typesetting the figures.

Protein extraction, digestion, and quantification

Eighty microliters of exosomes isolated from human plasma was ground with shock for 3× 400 s, lysed in ice-water bath for 30 min using a lysis solution (1% SDS, 8 M urea in water, and 1x Protease Inhibitor Cocktail), and centrifuged at 15,000 rpm for 15 min at 4°C to obtain the supernatant. One hundred micrograms of the extracted protein was adjusted to 100 μL of 8 M urea. Two microliters of 0.5 M tris(2-carboxyethyl) phosphine (TCEP) was added, followed by the addition of 4 μL of 1 M iodoacetamide. The reaction lasted 40 min at room temperature in dark. Then, 400 μL of precooled acetone was added for protein precipitation overnight at −20°C followed by centrifugation at 12,000 *g* for 20 min at 4°C. One milliliter of precooled acetone was added, vortexed, and then centrifuged as described earlier. After drying at room temperature, the precipitate was resuspended in 100 μL of 100 mM triethylamonium bicarbonate (TEAB). Trypsin (Promega, Madison, Wisconsin, United States) was added according to the mass ratio of enzyme to protein = 1:50 and hydrolyzed overnight at 37°C. Then, the concentration of the digested peptide was determined by the Pierce quantitative peptide assay kit (Thermo Scientific, San Jose, USA). The final peptides were desalted using a MonoSpin™ C18 column (GL Science Inc., Tokyo, Japan).

LC-MS/MS analysis

The peptides were redissolved in solvent A (A: 0.1% formic acid in water) and analyzed by an on-line nanoelectrospray LC-MS/MS using Orbitrap Fusion™ Lumos™ Tribrid™ (Thermo Fisher Scientific, MA, USA) coupled to EASY-nLC 1200 system (Thermo Fisher Scientific, MA, USA). Two microliters of peptide was loaded to an analytical column (Acclaim PepMap C18, 75 μm x 15 cm) and separated with a 60-min gradient, from 5% to 32% B (B: 0.1% formic acid in ACN). The column flow rate was maintained at 300 nL/min with the column temperature of 40°C. The electrospray voltage of 2 kV versus the inlet of the mass spectrometer was used. The mass spectrometer was run under data-dependent acquisition mode and automatically switched between MS and MS/MS mode. The parameters were as follows: (1) MS: scan range (*m/z*) = 350–1400; resolution = 120,000; AGC target = 5e5; maximum injection time = 50 ms; include charge states = 2–6; dynamic exclusion = 30 s; (2) HCD-MS/MS: resolution = 15,000; isolation window = 1.6; AGC target = 5e4; maximum injection time = 50 ms; collision energy = 28.

LC-MS/MS data were processed using PEAKS Studio version X+ (Bioinformatics Solutions Inc., Waterloo, Canada). PEAKS DB was set up to search Homo_sapiens_sp_201907 databases (20,414 entries) assuming trypsin as the digestion enzyme. PEAKS DB was searched with a fragment ion mass tolerance of 0.02 Da and a parent ion tolerance of 7 ppm. Carbamidomethylation (C) was specified as the fixed modifications. Oxidation (M) and acetylation (Protein N-term) were specified as the variable modifications. Peptides were filter by 1% false discovery rate (FDR). Proteins were identified with at least 1 unique peptide with 1% FDR.

GO enrichment

For an in-depth understanding of the identified significant proteins, GO enrichment was performed using DAVID (https://david.ncifcrf.gov/summary.jsp), an online bioinformatics tool for annotating the function of genes or proteins (Huang da et al., 2009). Briefly, the identified significant proteins were imported into the DAVID online database for reannotation. The parameters were as follows: 1) List: protein-coding gene names; 2) Identifier: official gene symbol; 3) Species: *Homo sapiens*. Then, the enrichment results of three

GO domains were obtained, including biological process (BP), molecular function (MF), and cellular component (CC) ($P < 0.05$). Finally, ggplot2 package (https://ggplot2.tidyverse.org/) in R was used to draw the bubble diagram to visualize the results.

ADDITIONAL RESOURCES

All studies are compliant with the relevant ethics approval for research. The informed consent was obtained from subjects for using the biological material for research purposes.

The study protocol was approved by the Ethics Committee of Ruijin Hospital as part of our longitudinal observational clinical research project registered at clinicalTrials.gov (trial ID: NCT03108677) (https://clinicaltrials.gov/ct2/results?recrs=&cond=&term=NCT03108677&cntry=&state=&city=&dist=) and is in accordance with relevant guidelines.